Demonstration of 4.7 kV Breakdown Voltage in NiO/β-Ga_2O_3 Vertical Rectifiers

Jian-Sian Li[1], Chao-Ching Chiang[1], Xinyi Xia[1], Timothy Jinsoo Yoo[2], Fan Ren[1], Honggyu Kim[2] and S.J. Pearton[2*]

[1] Department of Chemical Engineering, University of Florida, Gainesville, FL 32606 USA

[2] Department of Materials Science and Engineering, University of Florida, Gainesville, FL 32606 USA

Abstract

Vertical heterojunction NiO/β n-Ga_2O/n^+ Ga_2O_3 rectifiers employing NiO layer extension beyond the rectifying contact for edge termination exhibit breakdown voltages (V_B) up to 4.7 kV, with power figure-of-merits, V_B^2/R_{ON} of 2 GW·cm^{-2}, where R_{ON} is the on-state resistance (11.3 mΩ.cm^2). Conventional rectifiers fabricated on the same wafers without the NiO showed V_B values of 840 V and power figure-of-merit of 0.11 GW.cm^{-2}. Optimization of the design of the two-layer NiO doping and thickness and also the extension beyond the rectifying contact by TCAD showed the peak electric field at the edge of the rectifying contact could be significantly reduced. The leakage current density before breakdown was 144mA/cm^2, the forward current density was 0.8kA/cm^2 at 12 V, and the turn-on voltage was in the range 2.2-2.4 V compared to 0.8 V without NiO. Transmission electron microscopy showed sharp interfaces between the NiO and epitaxial Ga_2O_3 and a small amount of disorder from the sputtering process.

*Author to whom correspondence should be addressed: spear@mse.ufl.edu

There is significant current interest in development of wide and ultra-wide bandgap semiconductors for power electronics applications to overcome the high on-state resistances and limited power capabilities of Si-based electronics [1-10]. In Si-based power electronics, nearly 10% of electricity in the U.S. is wasted on power conversion and reducing these losses can help reduce reliance on fossil fueled power plants. The reduction of resistive losses and higher energy conversion efficiency of commercialized SiC and GaN can improve both the power density and efficiency of systems controlling power switching [1-7]. Further improvements in power figure-of-merit (FOM) should be possible with the ultra-wide bandgap semiconductors diamond, Ga_2O_3 and AlN [8-14]. In particular, there has been significant progress in monoclinic β-Ga_2O_3, which shows both materials [15-46] and economic [11] benefits and is commercially available in high quality large area substrate form using well-established melt crystal growth methods [9,10]. Lateral β-Ga_2O_3-based devices with breakdown voltage up to 8 kV [15] and critical breakdown fields exceeding the theoretical limits of SiC and GaN have been reported [15,32]. Vertical geometry devices are also attractive due to their larger current-carrying capability and breakdown voltages >2kV have been reported for β-Ga_2O_3 vertical rectifiers involving planar or trench Metal-Oxide-Semiconductor (MOS) approaches [20,47,48]. A recent report has demonstrated up to 6kV breakdown using a vertical structure with a deep trench of SiO_2 to provide edge termination [49].

With conventional, planar vertical geometry Ga_2O_3 rectifiers, the maximum electric field occurs at the edge of the rectifying contact and thermionic field emission-dominated leakage limits performance [22]. The electric field concentration at the edge of the gate electrode is several times higher than under the center region of the contact [8,9,30]. This has led to research on trench MOS approaches, where the maximum field occurs at the trench bottom and use of a

dielectric decreases the leakage current [8, 20, 22,29, 47]. A disadvantage is additional process complexity and reduced forward current density. Junction barrier Schottky (JBS) rectifiers have similar issues [9,47]. Irrespective of the edge-termination structure, the total length of termination along the surface plays a role in increasing the breakdown voltage [30]. Typically for SiC power devices, it is difficult to ensure high breakdown voltage and process robustness when the termination region is shorter than 3-5 times the thickness of the voltage-blocking layer [3,5].

The lack of shallow p-type dopants for β-Ga_2O_3 has created interest in integration of n-type Ga_2O_3 with p-type NiO for vertical p–n heterojunction power diodes [33.36-46]. These typically show smaller leakage current than conventional planar rectifiers and also have larger turn-on voltages [38-42]. The minority carrier nature of these devices should allow lower on-resistances and better on-state performance. Sputtered NiO_x is polycrystalline with a bandgap of ~ 3.7–4.0 eV and controllable p-type doping [50]. NiO/β-Ga_2O_3 JBS diodes with area 100 × 100 μm ^{2} have demonstrated V_B of 1715 V and R_{ON} of 3.45 mΩ·cm ^{2}, for a Baliga's figure of merit of 0.85 GW.cm $^{-2}$. The highest reported values are a static V_B of 2.41 kV [51] and specific on-resistance of 1.12 mΩ.cm^2, producing a FOM of 5.18 GW.cm^2 [51]. For larger devices, a JBS diode with area 1 × 1 mm ^{2} showed a forward current of 5A and breakdown voltage 700 V (FOM 64 MW/cm^2) [23]. For a 9-mm^2 heterojunction rectifier, a surge current of 45 A was recorded in a 10-ms surge transient [38]. Promising reliability was reported, with over 1-million times dynamic breakdown at a 1.2-kV peak overvoltage [42].

In this paper, we show that, with guidance from TCAD simulations in designing the NiO layer doping and thickness and extension beyond the rectifying contact, plus careful control of sputtering parameters, it is possible to achieve 4.7 kV V_B in vertical planar NiO/Ga_2O_3 rectifiers

and FOM of 2GW.cm^{-2}. These devices are processed without the complications of trench etching and subsequent dielectric deposition.

We first ran TCAD simulations from the Silvaco Atlas code to examine the effect of various device structures with and without NiO and then focused on differences between a single layer of NiO versus a bilayer. The latter was used to optimize contact resistance and field profiles. The NiO doping concentration (10^{15}-1x10^{19} cm^{-3}), thickness (10, 20, 40, 60, 80 nm) and single versus double layers at constant thickness were variables in both simulations and subsequent fabricated devices. The distance (1-15 μm) of a NiO guard ring from the rectifying contact was also simulated. According to our previous experiments, the energy bandgap and the hole mobility of NiO was set to be 3.8 eV and 0.5 cm^2 / V s, respectively. Based on the simulation results as guidance, we fabricated the structures I-IV that are shown schematically in Figure 1. By extending the NiO beyond the edge of the metal contact, simulations and subsequent experimental data showed this provided a type of guard ring effect, in spreading the electric field crowding at the edge of the diodes and thus structure II had superior breakdown voltages to structure I. While the electric field distributions of structure II and III were similar, experimentally, we found that a large area of NiO due to full extension of the conducting NiO to the edge of the device caused high leakage current. Structure IV did not improve the electric field in the TCAD simulation or in the experimental V_B. Figure S1 in the Supplemental Material shows more details in a schematic of the one- and two- NiO layer approaches, the metal and NiO thicknesses and the O_2/Ar sputtering ratios used to control the p-doping level in the NiO.

Based on guidance from the simulations, we then fabricated vertical rectifiers on structures consisting of a thick, lightly doped epitaxial layer on a conducting substrate. The drift region of the material consisted of a 10 μm thick, lightly Si doped epitaxial layer grown by halide vapor

phase epitaxy (HVPE) with carrier concentration $2x10^{16}$ cm^{-3}, grown on a (001) surface orientation Sn-doped β-Ga_2O_3 single crystal (Novel Crystal Technology, Japan). A full area Ti/Au backside Ohmic contact was formed by e-beam evaporation and was annealed at 550℃ for 1minute under N_2 ambient [48]. NiO was deposited by magnetron sputtering at 3mTorr and 150W of 13.56 MHz power using two separate targets operated at the same time to double the deposition rate to around 0.2 Å.sec^{-1}. Calibration of the doping and mobility were made from Hall measurements on thick layer (60 nm) of the NiO deposited on quartz. The Ar/O_2 ratio was used to control the doping in the NiO in the range $2x10^{18}$- 3 $x10^{19}$ cm^{-3}, with mobility < 1 $cm^2 \cdot V^{-1}$ s^{-1} and we used both single and double layers with two different doping concentrations, the first, lighter-doped layer on top of the Ga_2O_3 to enhance breakdown while a subsequent more heavily-doped layer on top of that was used to minimize contact resistance. The Ni/Au contact metal (100 μm diameter) was deposited onto the NiO layer after annealing at 300℃ under O_2 ambient. Compared to typical NiO thicknesses of 300 to 500 nm, we used ultra-thin layers. Previous simulations reported in the literature show that while the heterojunctions diodes will have higher turn-on voltage, they should exhibit higher reverse breakdown that conventional Schottky rectifiers [52].

The top layer NiO thickness was held constant at 10nm while the bottom layer of NiO thickness varied from 10 to 80 nm. The best simulation results (and subsequent experimental, results, as shown in the supplemental file, Table S1) were obtained on structure II, shown in Figure 2, which has the limited extension of the NiO beyond the rectifying contact to provide edge termination. To summarize the link between the TCAD simulation results and the experimental structures, (i) we found that a single layer of NiO always produced higher fields and lower simulated breakdown than a bi-layer when the latter structure was optimized to have

higher doping in the upper layer and lower doping in the layer directly on top of the Ga_2O_3. Increasing the doping concentration of NiO layer in contact with the Ni/Au electrode reduced the maximum electric field at the contact edge. Similarly, reducing the doping concentration of the lower NiO layer in contact with Ga_2O_3 also reduced field crowding, (ii) the extension of the NiO beyond the Ni/Au also increased breakdown voltage, but there was no improvement beyond an extension of 5µm (Figure S1), similar to the general trends reported for SiC rectifiers [3,5], (iii) increasing the thickness of the NiO was deleterious to breakdown beyond a total of 20 nm for the bi-layer, as the maximum field at the surface increased. The TCAD results were then used to guide the experimental device design.

A 20/80 nm Ni/Au Schottky contact was deposited with E-beam after lithographic patterning followed by standard acetone lift-off. Figure 2 also shows how the NiO is able to reduce the field at the edge of the rectifying contact, as predicted from the TCAD simulations. Those simulations also showed that the electric field decreases with lower doping concentrations and with smaller thickness, the electric field in NiO film increased while the electric field in the Ga_2O_3 decreased. However, this is also a function of doping and guidance on what to use experimentally was obtained from the simulations.

The current-voltage (I-V) characteristics were recorded with a Tektronix 370-A curve tracer, 371-B curve tracer and Agilent 4156C was used for forward and reverse current measurements over the temperature range 300-600K on a temperature-controlled stage. The forward direction was dominated by the thermionic emission (TE) current, while in the reverse direction, the thermionic field emission (TFE) and tunneling currents played an important role at high reverse bias [53,54]. The reverse breakdown voltage was defined as the bias for a reverse current reaching 0.1 $A.cm^2$, which has been standard for previous studies [42,51]. Many devices (5-

10) were measured for each design and typically showed V_B values within a few percent of each other within an area of 0.5 cm^2. The breakdown values were overwhelmingly repeatable and only a few tests (around 5%) resulted in destructive reverse breakdown. This is consistent with our previous observations [14,24,26], in that edge terminated devices are much more robust than unterminated rectifiers.

For transmission electron microscopy (TEM) imaging, cross-section TEM samples of the NiO/β-Ga_2O_3 heterostructures were prepared along the [100] zone axis (β-Ga_2O_3) using a FEI Helios Dualbeam Nanolab 600 focused ion beam (FIB) system. High resolution TEM (HRTEM) imaging of the NiO/β-Ga_2O_3 interface structure was carried out using a 200 kV Talos F200i (Thermo Scientific) equipped with a Ceta 16M camera. Typical images are shown in Figure 3. Figure 3 (a) shows a HRTEM image of the full diode structure, consisting of the top electrode (Au, Ni), p-type NiO, and n-type β-Ga_2O_3 from top to bottom, recorded along [100] projection with respect to β-Ga_2O_3. Near-surface damage is present within the top 10 nm of the Si-doped β-Ga_2O_3 layer, as evidenced by the image contrast change in Figure 3 (a). This is likely due to the energetic sputtering process for the NiO overlayer. However, high magnification HRTEM image in Figure 3 (b) demonstrates that the NiO/β-Ga_2O_3 interface is atomically abrupt and the β-Ga_2O_3 near the heterointerface is fairly pristine with the absence of extended defects (e.g., dislocations).

The reverse I-V characteristics from a selection of rectifiers is shown in Figure 4. These were measured in Fluorinert atmosphere at 25°C. The experimental values of breakdown and on-resistance for single layer and double layer NiO structures are shown in Table S1 in the supplementary data. The double layer structures exhibited much larger breakdown voltages than the dingle layer structures, showing the benefit of optimizing the field profile. The maximum value of ~4.7 kV was obtained for a 2-layer NiO structure with respective thicknesses of 10/10

nm and the respective doping of 2.6 x10^{19}/3.5x10^{18} cm^{-3}. Increasing the thickness of the NiO reduced the V_B and was 2.5 kV for 80 nm NiO. This is consistent with the improved performance of other devices using thinner NiO [51]. The metal gate rectifier without NiO showed a V_B of ~840 V for this contact dimension of 100 µm. The maximum value of V_B for the heterojunction rectifier is about twice that reported previously [51], and the data suggests that even higher values could be obtained with further optimization. For the other device designs, for structure I, the V_B was < 2 kV in all cases, while for structure III, the leakage current was large (> 1mA/cm^2 at -100V). For the structure IV, the V_B was similar to that of the simple NiO layer extension and the added guard rings made no improvement. The simplicity of the optimized device design and straightforward processing without the need for trenches makes this an attractive option.

The forward I-V characteristics are shown in Figure 5 for the heterojunction rectifiers with different NiO thickness. Compared to the turn-on voltage of 0.8V for the conventional metal rectifier, those for the heterojunctions are in the range 2.2-2.4 V, but with similar current densities at these higher forward biases. The leakage current density before breakdown was 144mA/cm^2, the forward current density was 0.8kA/cm^2 at 12 V. Table I shows a compilation of the R_{ON} and power figure-of-merit values for the conventional rectifier and for the heterojunction rectifiers with different thicknesses of NiO. While the R_{ON} values for the latter are slightly higher than for the conventional rectifier, optimization of the doping/thickness of the NiO can minimize this difference [51]. In our case, the lateral spread resistance of the NiO layer for 20 nm thickness is ~10^4 Ω, significantly larger than the device on-resistance. This means there is insignificant lateral expansion of the conductive area for this device design. The power figure-of-merit of 2 GW.cm^{-2} is still well short of the theoretical maximum of ~34 GW.cm^{-2} and

shows there is still room to optimize the edge termination and defect density in the drift layer. Figure 6 shows the on-state resistances and forward current densities for these same devices, with current densities > 10 A.cm^{-2} even at relatively low bias.

Figure 7 shows a compilation of R_{on} versus V_B results reported in the literature for conventional Schottky barrier or JBS rectifiers and NiO/Ga_2O_3 heterojunction rectifiers, along with the theoretical lines for different wide bandgap and ultra-wide bandgap semiconductors. The present work shows the potential of Ga_2O_3 to achieve values comparable to the limits of GaN and SiC. Future work should continue to focus on defect reduction in the Ga_2O_3 epi layers, low damage edge termination methods, transition to larger device areas and the reliability of devices under realistic operating conditions.

In summary, we present a double-layer NiO/β-Ga_2O_3 p-n heterojunction diode, which exhibits high performance breakdown voltage and low on-resistance. Through design of the ultra-thin (20 nm) double-layer NiO structure, the V_B is substantially improved to 4.7 kV with R_{on} of 11.3 mΩ·cm^2 and a figure-of-merit (V_b^2/R_{on}) of 2 GW.cm^{-2}. The high V_B is attributed to the structure of both the double-layer and the NiO extension to provide edge termination. From the TCAD simulation, the peak of the electric field is located at the edge of the diodes. Increasing the doping concentration of the NiO layer contacting Ni/Au can reduce the electric field at the edge of the Ohmic contact. Simultaneously, the low doping concentration of the NiO contact with β-Ga_2O_3 can move the electric field maximum from the edge to the inside of devices. In addition, the extension guard ring can also reduce the electric field crowding. This work provides a desirable design strategy for NiO/Ga_2O_3 structures, leading to the highest breakdown voltage among all Ga_2O_3-based p-n diodes.

Acknowledgments

The work at UF was performed as part of Interaction of Ionizing Radiation with Matter University Research Alliance (IIRM-URA), sponsored by the Department of the Defense, Defense Threat Reduction Agency under award HDTRA1-20-2-0002. The content of the information does not necessarily reflect the position or the policy of the federal government, and no official endorsement should be inferred. The work at UF was also supported by NSF DMR 1856662 (James Edgar).

Data Availability

The data that supports the findings of this study are available within the article and its supplementary material.

Declarations

The authors have no conflicts to disclose

Supplementary Material

See supplementary material for details on device structures and process parameters.

References

1. H. Fu, K. Fu, S. Chowdhury, T. Palacios and Y. Zhao, IEEE Trans Electron Dev., 68, 3200 (2021).

2. H. Fu, K. Fu, S. Chowdhury, T. Palacios and Y. Zhao, IEEE Trans Electron Dev, 68, 3212 (2021)

3. J. Ballestín-Fuertes, J. Muñoz-Cruzado-Alba, J. F. Sanz-Osorio, E. Laporta-Puyal, Electronics, 10, 677 (2021).

4. Y. Zhang and T. Palacios, IEEE Trans Electron Dev, 67, 3960 (2020).

5. J.Y. Tsao, S. Chowdhury, M.A. Hollis, D. Jena, N.M. Johnson, K.A. Jones, R.J. Kaplar, S. Rajan, C.G. Van de Walle, E. Bellotti, C.L. Chua, R. Collazo, M.E. Coltrin, J.A. Cooper, K.R. Evans, S. Graham, T.A. Grotjohn, E.R. Heller, M. Higashiwaki, M. S. Islam, P.W. Juodawlkis, M.A. Khan, A.D. Koehler, J.H. Leach, U.K. Mishra, R.J. Nemanich, R. Pilawa-Podgurski, J.B. Shealy, Z. Sitar, M.J. Tadjer, A.F. Witulski, M. Wraback and J.A. Simmons, Adv. Electron. Mater. 4, 1600501 (2018).

6. Y. Sun, X. Kang, Y. Zheng, J. Lu, X. Tian, K. Wei, H. Wu, W. Wang, X. Liu and G. Zhang, Electronics, 8, 575 (2019).

7. Matteo Meneghini, Carlo De Santi, Idriss Abid, Matteo Buffolo, Marcello Cioni, Riyaz Abdul Khadar, Luca Nela, Nicolò Zagni, Alessandro Chini, Farid Medjdoub, Gaudenzio Meneghesso, Giovanni Verzellesi, Enrico Zanoni and Elison Matioli, J. Appl. Phys.130, 181101 (2021).

8. M. H. Wong and M. Higashiwaki, IEEE Trans Electron Dev, 67, 3925 (2020).

9. Andrew J. Green, James Speck, Grace Xing, Peter Moens, Fredrik Allerstam, Krister Gumaelius, Thomas Neyer, Andrea Arias-Purdue, Vivek Mehrotra, Akito Kuramata, Kohei

Sasaki, Shinya Watanabe, Kimiyoshi Koshi, John Blevins, Oliver Bierwagen, Sriram Krishnamoorthy, Kevin Leedy, Aaron R. Arehart, Adam T. Neal, Shin Mou, Steven A. Ringel, Avinash Kumar, Ankit Sharma, Krishnendu Ghosh, Uttam Singisetti, Wenshen Li, Kelson Chabak, Kyle Liddy, Ahmad Islam, Siddharth Rajan, Samuel Graham, Sukwon Choi, Zhe Cheng, and Masataka Higashiwaki, APL Mater. 10, 029201 (2022).

10. S. J. Pearton, Fan Ren, Marko Tadjer and Jihyun Kim, J. Appl. Phys. 124, 220901 (2018).

11. Samantha B. Reese, Andriy Zakutayev, Proc. SPIE 11281, Oxide-based Materials and Devices XI, 112810H (2020).

12. Chenlu Wang, Jincheng Zhang, Shengrui Xu, Chunfu Zhang, Qian Feng, Yachao Zhang, Jing Ning, Shenglei Zhao, Hong Zhou and Yue Hao, J. Phys. D: Appl. Phys. 54, 243001 (2021).

13. S. Sharma, K. Zeng, S. Saha, U. Singisetti, IEEE Electron Dev. Lett. 41, 6 836 (2020).

14. Jiancheng Yang, F. Ren, Marko Tadjer, S. J. Pearton and A. Kuramata, AIP Adv. 8, 055026 (2018).

15. S. Roy, A. Bhattacharyya, P. Ranga, H. Splawn, J. Leach and S. Krishnamoorthy, IEEE Electron Dev. Lett. 42, 1140 (2021).

16. X. Lu, X. Zhou, H. Jiang, K. W. Ng, Z. Chen, Y. Pei, K. M. Lau, and G. Wang, IEEE Electron Dev Lett. 41, 449 (2020).

17. B. Chatterjee, K. Zeng, C. D. Nordquist, U. Singisetti and S. Choi, IEEE Trans. Compon, Packaging Man Technol, 9, 2352 (2019).

18. K. D. Chabak, K. D. Leedy, A. J. Green, S. Mou, A. T Neal, T. Asel, E. R. Heller, N. S. Hendricks, K. Liddy, A. Crespo, N. C. Miller, M. T. Lindquist, N. Moser, R. C. Fitch Jr, D. E. Walker Jr, D. L Dorsey and G. H. Jessen, Semicond Sci Technol, 35, 013002 (2020).

19. Zongyang Hu, Kazuki Nomoto, Wenshen Li, Zexuan Zhang, Nicholas Tanen, Quang Tu Thieu, Kohei Sasaki, Akito Kuramata, Tohru Nakamura, Debdeep Jena, and Huili Grace Xing, Appl. Phys. Lett. 113, 122103 (2018).

20. W. Li, K. Nomoto, Z. Hu, D. Jena and H. G. Xing, IEEE Electron Dev. Lett, 41, 107 (2020).

21. Ribhu Sharma, Minghan Xian, Chaker Fares, Mark E. Law, Marko Tadjer, Karl D. Hobart, Fan Ren and Stephen J. Pearton, J. Vac. Sci. Technol A 39, 013406 (2021).

22. Wenshen Li, Devansh Saraswat, Yaoyao Long, Kazuki Nomoto, Debdeep Jena, and Huili Grace Xing, Appl. Phys. Lett. 116, 192101 (2020)

23. Y. Lv, Y. Wang, X. Fu , Shaobo Dun, Z. Sun, Hongyu Liu, X. Zhou, X. Song, K. Dang, S. Liang, J. Zhang, H. Zhou, Z. Feng, S. Cai and Yue Hao, IEEE Trans Power Electron. 36, 6179 (2021).

24. Jiancheng Yang, Minghan Xian, Patrick Carey, Chaker Fares, Jessica Partain, Fan Ren, Marko Tadjer, Elaf Anber, Dan Foley, Andrew Lang, James Hart, James Nathaniel, Mitra L. Taheri, S. J. Pearton and Akito Kuramata, Appl. Phys. Lett. 114, 232106 (2019)

25. Z. Jian, S. Mohanty, and E. Ahmadi,Appl. Phys. Lett., 116, 152104 (2020).

26. J. Yang, F. Ren, Y.-T. Chen, Y.-T. Liao, C.-W. Chang, J. Lin, M. J.Tadjer, S. J. Pearton, and A. Kuramata, IEEE J. Electron Dev. Soc., 7, 57 (2019).

27. T. Harada, and A. Tsukazaki, Appl. Phys. Lett., 116, 232104 (2020).

28. C. -H. Lin, Y. Yuda, M. H. Wong, M. Sato, N. Takekawa, K. Konishi, T. Watahiki, M. Yamamuka, H. Murakami, Y. Kumagai and Masataka Higashiwaki, IEEE Electron Dev. Lett., 40, 1487 (2019).

29. W. Xiong, X. Zhou, G. Xu, Q. He, G. Jian, C. Chen, Y. Yu, W. Hao, X. Xiang, X. Zhao, W. Mu, Z. Jia, X. Tao, and S. Long, IEEE Electron. Dev. Lett.42, 430 (2021).

30. S. J. Pearton, J. Yang, P. H. Cary, F. Ren, J. Kim, M. J. Tadjer and M. A. Mastro,Appl. Phys. Rev., 5, 011301 (2018).

31. Ming Xiao, Boyan Wang , Jingcun Liu , Ruizhe Zhang, Zichen Zhang, Chao Ding, Shengchang Lu, Kohei Sasaki, Guo-Quan Lu, Cyril Buttay, and Yuhao Zhang, IEEE Trans. Power Electron. 36, 8565 (2021).

32. Arkka Bhattacharyya, Shivam Sharma, Fikadu Alema, Saurav Roy, Carl Peterson, George Seryogin, Andrei Osinsky, Uttam Singisetti, Sriram Krishnamoorthy, Appl. Phys. Expr (in press, 2022)

33. X. Lu, Xianda Zhou, Huaxing Jiang, Kar Wei Ng, Zimin Chen, Yanli Pei, Kei May Lau and Gang Wang, IEEE Electron Dev. Lett.41, 449 (2020).

34. Chenlu Wang, Hehe Gong, Weina Lei, Y. Cai, Z. Hu, Shengrui Xu, Zhihong Liu , Qian Feng , Hong Zhou, Jiandong Ye, Jincheng Zhang, Rong Zhang, and Yue Hao, IEEE Electron Dev. Lett, 42, 485 (2021).

35. S. Roy , A. Bhattacharyya , P. Ranga , H. Splawn, J. Leach, and S. Krishnamoorthy, IEEE Electron Device Lett., 42, 1540 (2021).

36. Qinglong Yan, Hehe Gong, Jincheng Zhang, Jiandong Ye, Hong Zhou, Zhihong Liu, Shengrui Xu, Chenlu Wang, Zhuangzhuang Hu, Qian Feng, Jing Ning, Chunfu Zhang, Peijun Ma, Rong Zhang, and Yue Hao, Appl. Phys. Lett. 118, 122102 (2021).

37. H. H. Gong, X. H. Chen, Y. Xu, F.-F. Ren, S. L. Gu and J. D. Ye, Appl. Phys. Lett., 117, 022104 (2020).

38. Hehe Gong, Feng Zhou , Weizong Xu , Xinxin Yu , Yang Xu, Yi Yang, Fang-fang Ren, Shulin Gu, Youdou Zheng, Rong Zhang, Hai Lu and Jiandong Ye, IEEE Trans. Power Electron., 36, 12213 (2021).

39. H. H. Gong, X. X. Yu, Y. Xu, X. H. Chen, Y. Kuang, Y. J. Lv, Y. Yang, F.-F. Ren, Z. H. Feng, S. L. Gu, Y. D. Zheng, R. Zhang, and J. D. Ye , Appl. Phys. Lett. 118, 202102 (2021)

40. H. H. Gong, X. H. Chen, Y. Xu, Y. T. Chen, F. F. Ren, B. Liu, S. L. Gu, R. Zhang, and J. D. Ye, IEEE Trans. Electron Dev. 67, 3341 (2020).

41. W. Hao, Q. He, K. Zhou, G. Xu, W. Xiong, X. Zhou, G. Jian, C. Chen, X. Zhao, and S. Long, Appl. Phys. Lett., 118, 043501 (2021).

42. F. Zhou, Hehe Gong, Weizong Xu, Xinxin Yu, Yang Xu, Yi Yang, Fang-fang Ren, Shulin Gu, Youdou Zheng, Rong Zhang, Jiandong Ye and Hai Lu, IEEE Trans. Power Electron, 37, 1223 (2022)

43. Qinglong Yan, Hehe Gong, Jincheng Zhang, Jiandong Ye, Hong Zhou, Zhihong Liu, Shengrui Xu, Chenlu Wang, Zhuangzhuang Hu, Qian Feng, Jing Ning, Chunfu Zhang, Peijun Ma, Rong Zhang, and Yue Hao, Appl. Phys. Lett. 118, 122102 (2021).

44. Qinglong Yan, Hehe Gong, Hong Zhou, Jincheng Zhang, Jiandong Ye, Zhihong Liu, Chenlu Wang, Xuefeng Zheng, Rong Zhang, and Yue Hao, Appl. Phys. Lett. 120, 092106 (2022).

45. Y. J. Lv, Y. G. Wang, X. C. Fu, S. B. Dun, Z. F. Sun, H. Y. Liu, X. Y. Zhou, X. B. Song, K. Dang, S. X. Liang, J. C. Zhang, H. Zhou, Z. H. Feng, S. J. Cai, and Y. Hao, IEEE Trans. Power Electron. 36, 6179 (2021).

46. Jiaye Zhang, Shaobo Han, Meiyan Cui, Xiangyu Xu, Weiwei Li, Haiwan Xu, Cai Jin, Meng Gu, Lang Chen and Kelvin H. L. Zhang, ACS Appl. Electron. Mater. 2, 456 (2020).

47. Gallium oxide vertical transistor with the world's highest breakdown voltage, press release Novel Crystal Technology, June 16, 2021, https://www.novelcrystal.co.jp/eng/2021/911/

48. Jiancheng Yang, Fan Ren, Marko Tadjer, S.J. Pearton and A Kuramata, ECS J. Solid State Sci. Technol.7, Q92 (2018).

49. Pengfei Dong, Jincheng Zhang, Qinglong Yan, Zhihong Liu, Peijun Ma, Hong Zhou, and Yue Hao, IEEE Electron. Dev. Lett. (in press, 2022).

50. J.A. Spencer, A.L. Mock, A.G. Jacobs, M. Schubert, Y. Zhang and M.J. Tadjer, Appl. Phys. Rev. 9, 011315 (2022).

51. Yuangang Wang, Hehe Gong, Yuanjie Lv , Xingchang Fu, Shaobo Dun, Tingting Han, Hongyu Liu, Xingye Zhou, Shixiong Liang, Jiandong Ye, Rong Zhang, Aimin Bu, Shujun Cai and Zhihong Feng, IEEE Trans. Power Electron. 37, 3743 (2022).

52. Hong Zhou, Shifan Zeng, Jincheng Zhang, Zhihong Liu, Qian Feng, Shengrui Xu, Jinfeng Zhang and Yue Hao, Crystals 11, 1186 (2021).

53. W. Li, D. Jena, and H. G. Xing, J. Appl. Phys. 131, 015702 (2022).

54. Swarnav Mukhopadhyay, Luke A. M. Lyle, Hridibrata Pal, Kalyan K. Das, Lisa M. Porter, and Biplab Sarka, J. Appl. Phys.131, 025702 (2022).

Table 1. Summary of conventional Ga_2O_3 and heterojunction NiO/Ga_2O_3 rectifiers. The thickness of the two NiO layers in nm is shown.

Parameter	**Ga_2O_3**	**NiO (10/10)**	**NiO (20/10)**	**NiO (40/10)**	**NiO (80/10)**
V_B (V)	840	4767	3095	3840	2543
R_{ON} ($m\Omega \cdot cm^2$)	6.7	11.3	12.5	7.6	6.6
V_B^2/R_{ON} ($GW \cdot cm^{-2}$)	0.11	2.01	0.77	1.95	0.98

Figure Captions

Figure 1. Different structures simulated in the TCAD program. These included extent of NiO extension beyond the rectifying contact, width and separation of NiO guard ring from rectifying contact, thickness and doping in NiO and one layer versus two layers of NiO with different doping in each. Based on the TCAD, structures I, II and III were then fabricated, with different thicknesses of the NiO layers.

Figure 2 (a) Schematic of the optimized NiO/Ga_2O_3 heterojunction rectifier.(b) TCAD simulations showing the reduction in electric field in the Ga_2O_3 at the edge of the contact with the NiO.

Figure 3. (a) Low magnification HRTEM image of the NiO/ β-Ga_2O_3 heterostructure with the top Au/Ni electrode. (b) High magnification HRTEM image of the interface between NiO and β-Ga_2O_3, showing the sharp interface. Structural damage near the surface of β-Ga_2O_3, marked by the blue arrows in (a-b), is observed that is evidenced by the image contrast change. This damage is likely induced by the energetic deposition process of the NiO overlayer, while the β-Ga_2O_3 top layer is pristine otherwise as shown in (b).

Figure 4. Reverse I-V characteristics from conventional Ga_2O_3 and double NiO layer NiO/Ga_2O_3 heterojunction rectifiers in which the top, heavily doped NiO thickness was constant at 10 nm while the lower, lighter doped NiO was varied from 10-80 nm. The arrows mark where breakdown occurs, to guide the eye. This is slightly different than the definition used to standardize V_B.

Figure 5. Forward I-V characteristics from conventional Ga_2O_3 and double layer NiO/Ga_2O_3 heterojunction rectifiers with different NiO thicknesses.

Figure 6. Log plot of forward current densities and R_{ON} values from conventional Ga_2O_3 and double layer NiO/Ga_2O_3 heterojunction rectifiers with different NiO thicknesses.

Figure 7. Compilation of. Ron versus V_B of conventional and NiO/Ga_2O_3 heterojunction rectifiers reported in the literature.

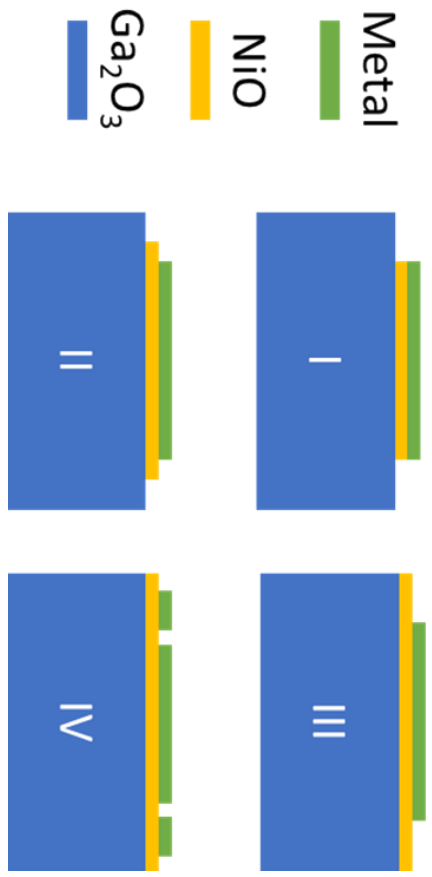

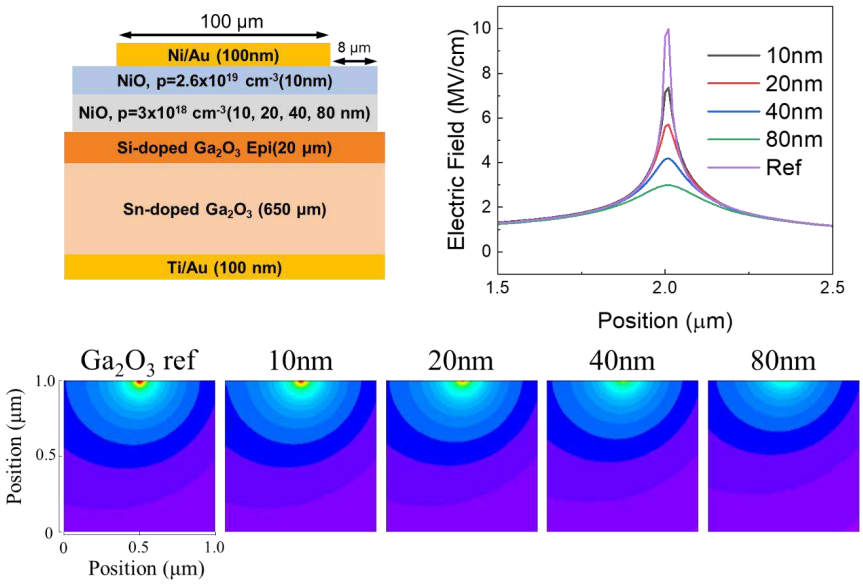

PLEASE CITE THIS ARTICLE AS DOI: 10.1063/5.0097564

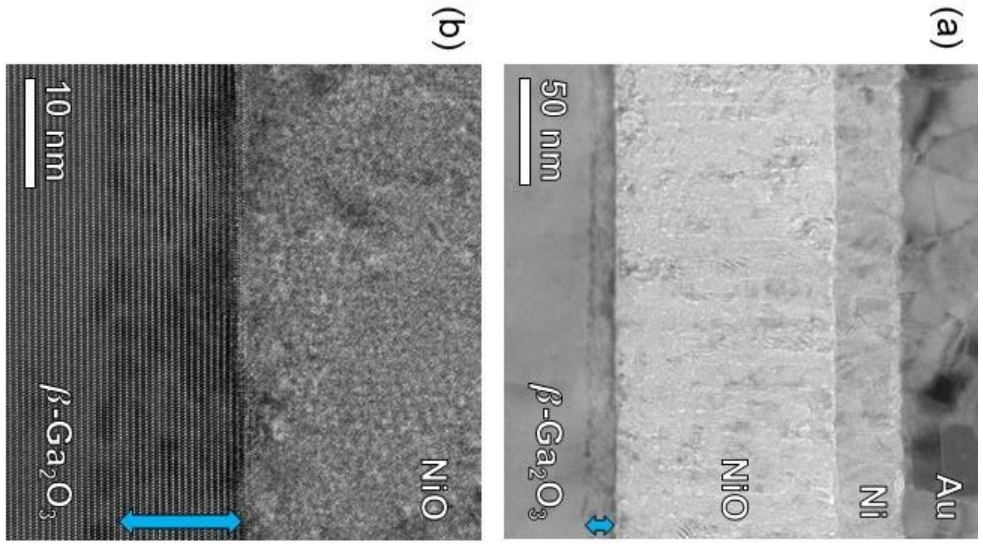

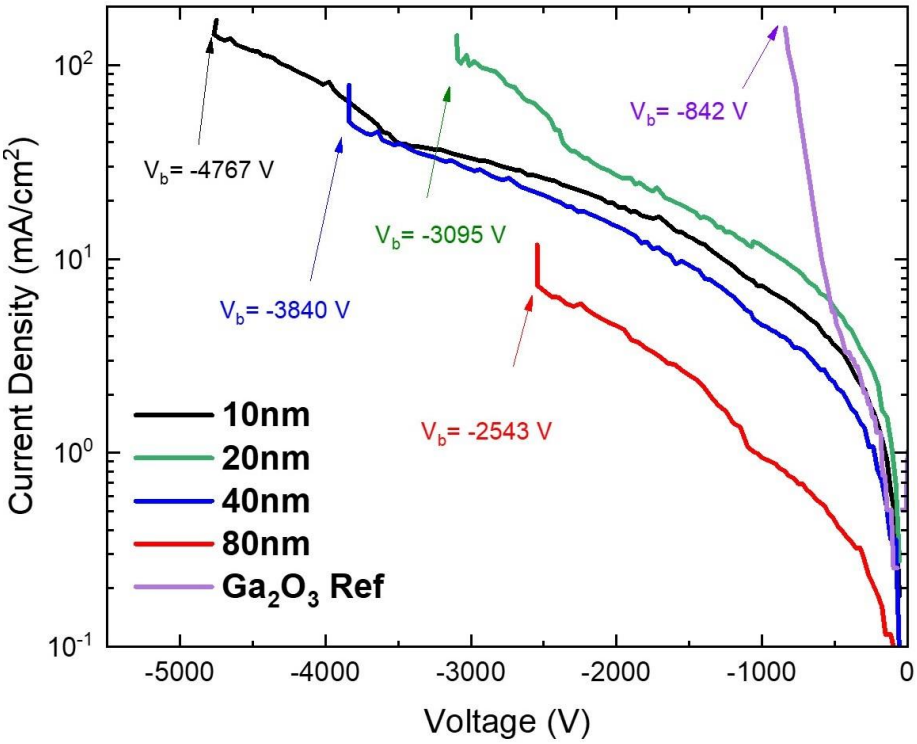

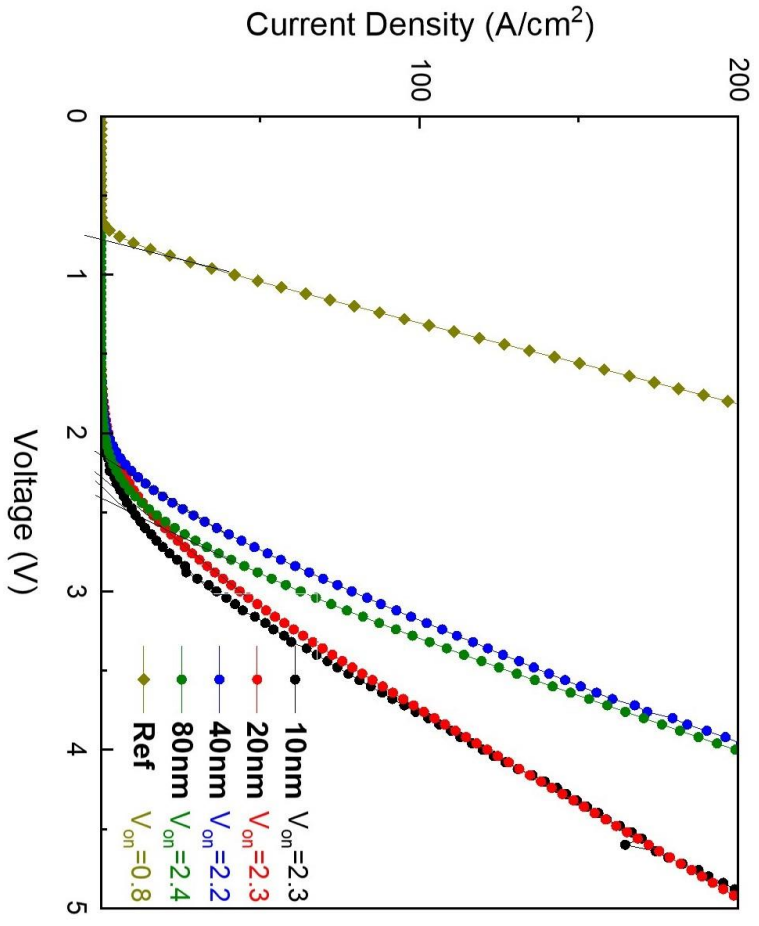

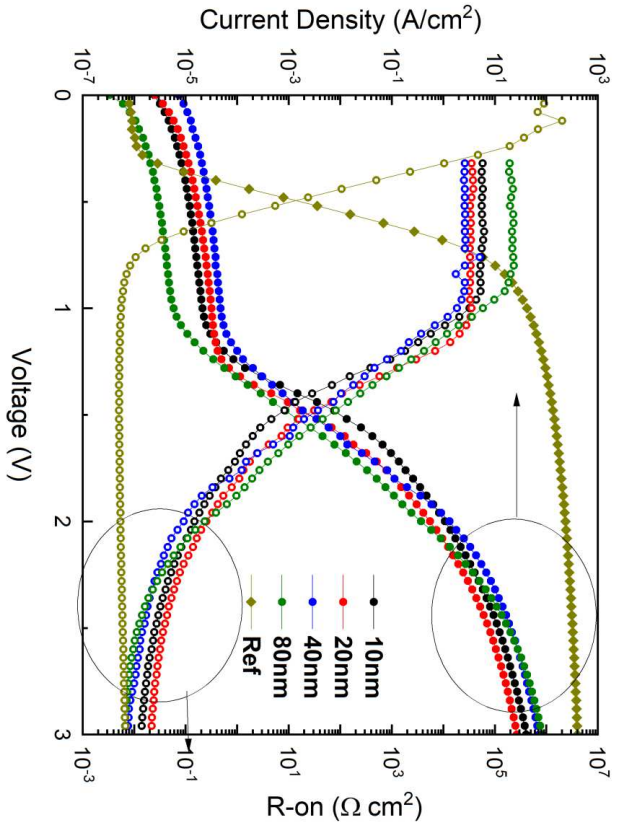

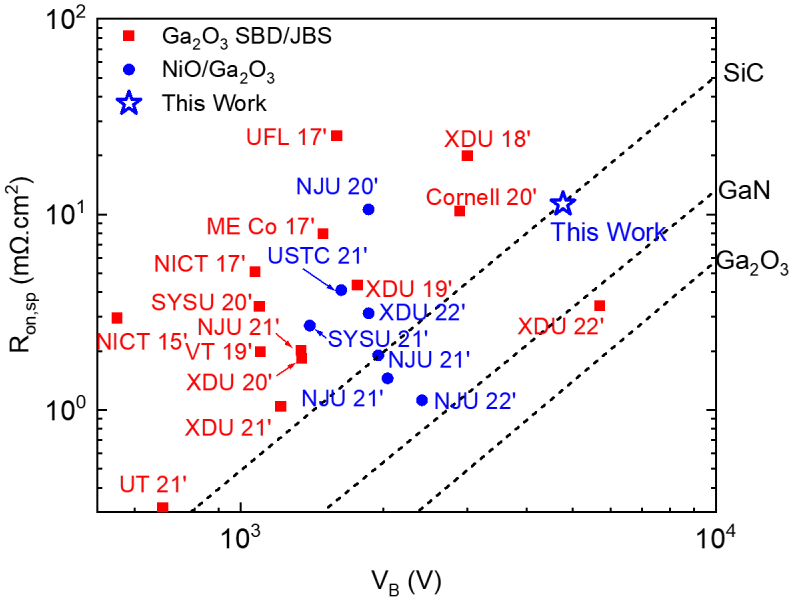

PLEASE CITE THIS ARTICLE AS DOI: 10.1063/5.0097564

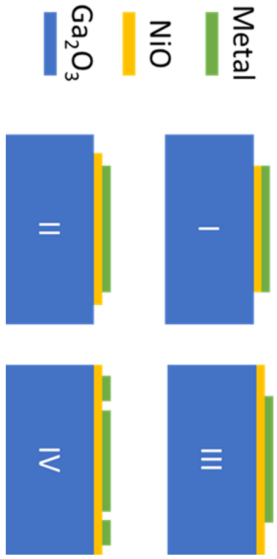

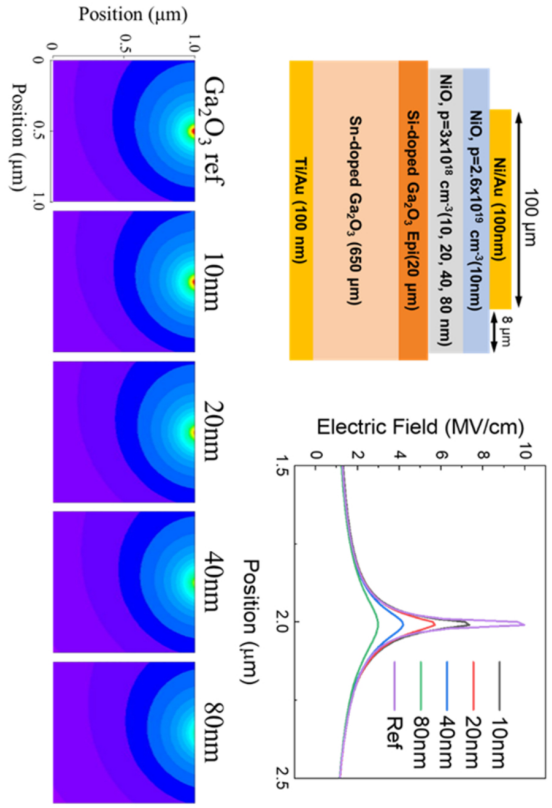

PLEASE CITE THIS ARTICLE AS DOI: 10.1063/5.0097564

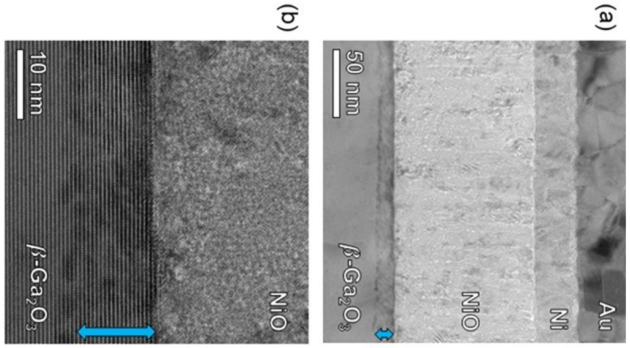

PLEASE CITE THIS ARTICLE AS DOI: 10.1063/5.0097564

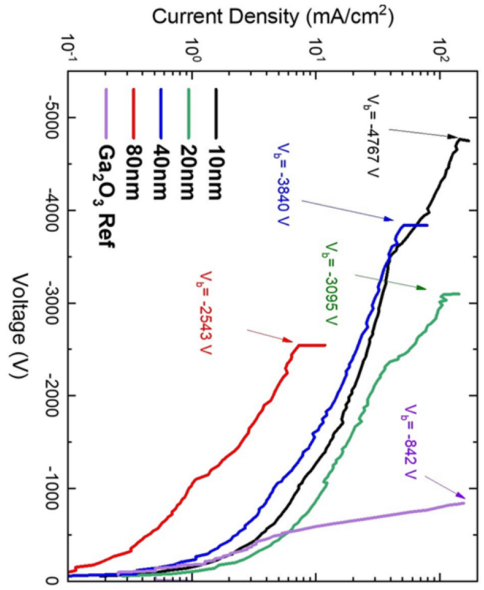

PLEASE CITE THIS ARTICLE AS DOI: 10.1063/5.0097564

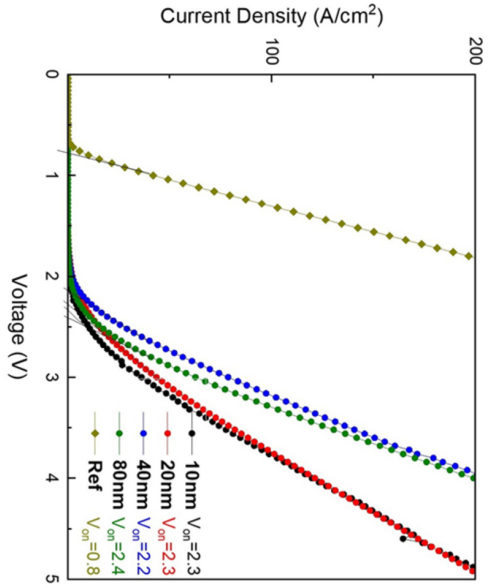

PLEASE CITE THIS ARTICLE AS DOI: 10.1063/5.0097564

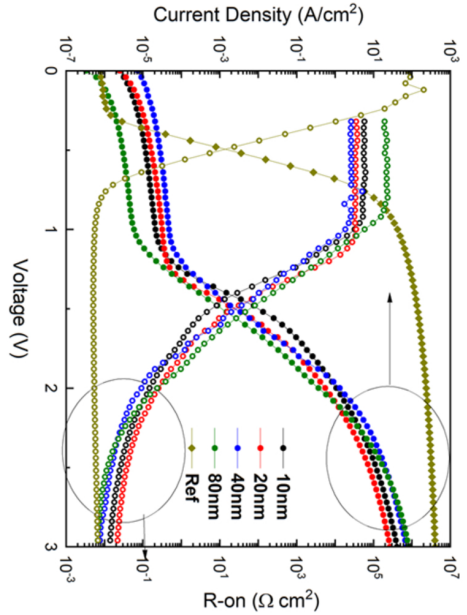

PLEASE CITE THIS ARTICLE AS DOI: 10.1063/5.0097564